Supporting Information

DNA nanostructure-programmed like-charge attraction at the cell-membrane interface

Hongming Ding,[○,†,§] Jiang Li,[○,‡] Nan Chen,[‡] Xingjie Hu,[‡] Xiafeng Yang,[‡] Linjie Guo,[‡] Qian Li,[‡] Xiaolei Zuo,[‡,∥] Lihua Wang,[‡] Yuqiang Ma,[*,†] and Chunhai Fan[*,‡]

[†]National Laboratory of Solid State Microstructures and Department of Physics, Collaborative Innovation Center of Advanced Microstructures, Nanjing University, Nanjing 210093, China;

[‡]Division of Physical Biology and Bioimaging Center, CAS Key Laboratory of Interfacial Physics and Technology, Shanghai Institute of Applied Physics, Chinese Academy of Sciences, Shanghai 201800, China;

[§]Center for Soft Condensed Matter Physics and Interdisciplinary Research, School of Physical Science and Technology, Soochow University, Suzhou 215006, China;

[∥]Institute of Molecular Medicine, Renji Hospital, Schools of Medicine and Chemistry and Chemical Engineering, Shanghai Jiao Tong University, Shanghai 200127, China

[*]Corresponding Authors: myqiang@nju.edu.cn; fchh@sinap.ac.cn

Materials and Methods:

Preparation and characterization of DNA nanostructures

All oligonucleotides purified with high-performance liquid chromatography (HPLC) were obtained from Invitrogen (Shanghai, China), and the sequences are shown in Table S1. TDN-13, TDN-20, and TDN32 were synthesized using the previously reported method[1]. In detail, four component oligonucleotides (listed in Table S1, 1 μM each) were mixed in equimolar quantities in TM buffer (10 mM of Tris and 5

mM of $MgCl_2$, pH =8.0). The mixture was heated to 95 °C for 5 min and then cooled to 4 °C in 30 sec. To synthesize TDN-20d, two TDN-20 monomers incorporated with T20 or A20 linker (at the 5' end of TDN-20-S1 in Table S1) were separately synthesized and HPLC purified, and were then mixed in equimolar ratio for 15-min incubation at room temperature (RT). The method to synthesize 6-helix was adapted from a previous report [2]. In detail, all 20 component oligonucleotides (listed in table S1, 1 μM each) were mixed in 200 μL TAE buffer (40 mM Tris, 20 mM acetic acid, 2 mM EDTA, and 125 mM magnesium acetate, with pH adjusted to 8.0). This mixture was then slowly cooled down from 95 °C to RT in water bath (in a 1L styrofoam box).

Cell culture

HeLa cells were obtained from Shanghai Institute of Biological Sciences, and were cultured in a 5% CO_2 environment at 37 °C in Dulbecco's modified Eagle's medium (DMEM, Invitrogen) and supplemented with 10% (vol/vol) fetal bovine serum (FBS) (Gibico), 100 international units/ml penicillin, 100 mg/ml streptomycin (Invitrogen) and 2 mM L-glutamine (Invitrogen). For fluorescence imaging, HeLa cells were cultured in 35-mm glass-bottom culture dishes (Shengyou biotechnology). To stain the cell membrane, the cells were incubated with 10 μg/mL DiO (Vybrant, ThermoFisher) for 15min; to stain the cell nucleus, the cells were treated with 5 μg/mL Hoechst33258 (Invitrogen) for 15 min, followed by thorough washing with PBS. For flow cytometry experiments, cells were seeded on 24-well culture plates at a density of 8×10^4 cells/mL and cultured for 24 h. For all subsequent experiments, the cells were washed with PBS 3 times and then stored in the fresh medium.

Treatments of cells with inhibitors and DNA nanostructures

To study the endocytosis pathway, the cells were pre-incubated with 5 mg/ml chlorpromazine (CPZ) or 7 mM methyl-β-cyclodextrin (mβCD) for 30 min, respectively. Then they were incubated with 50 nM Cy3-labeled TDN-20 for 6h. The inhibitors were maintained in the cell culture medium throughout the experiments. HeLa cells were incubated with Cy3-labeled DNA nanostructures (50 nM) for 6 h, and incubated with 50 nM Cy3-lebeled DNA nanostructures for imaging.

Cell synchronization

The procedure for cell cycle synchronization method was adapted from the previously reported method[3]. Briefly, to obtain G0/G1 Phase enriched cell cultures，we washed the HeLa cells with PBS buffer three times and then incubated them in FBS-free DMEM for 48 h. To obtain S phase enriched cells, the cells were firstly incubated in DMEM containing 2 mM thymidine (Sigma-M1404) for 20 h, then in normal fresh medium for 10 h，and subsequently incubated in thymidine-containing DMEM for another 20 h. For G2/M phase synchronization, the HeLa cells were incubated in DMEM with 2 mM thymidine for 24 h, then in normal DMEM for 3 h for releasing, which afterwards were incubated in DMEM containing 400 ng/mL nocodazole (Sigma-M1404) for 24 h.

Induction of cell autophagy

Induction of autophagy with rapamycin has been previously described[4]. Briefly, we incubated HeLa cells with 5 μM of rapamycin in FBS-containing culture medium for 24 h followed by washing with PBS, 6 h incubation with the DNA nanostructures in FBS-free culture medium containing 5 μM of rapamycin.

Fluorescence microscopic imaging

Confocal images were obtained using a Leica TCS SP8 confocal microscope. Cy3-labeled DNA structures were excited with a 561 nm helium-neon laser; DiO-labeled lipid was excited with a 488nm Ar–Kr laser; Hoechst33258-labeled nuclei were excited with a 405nm diode laser. The imaging channels were 570-630, 500-550, and 450-500 nm correspondingly. All images were shown in pseudo colors for better contrast. The fluorescence emission was collected using an NA = 1.40, 63× oil immersion objective. To construct the 3D image, successive z-stacks spaced by 1.2 μm were recorded. The XY imaging plane is located approximately 3 μm above the bottom of the cells. For time-lapse fluorescence imaging of living cells, cells were plated in 35 mm glass bottom dish and transfected 24 h before imaging, and were maintained at 37 ºC in a live cell incubator during observation. Videos were made from time lapse images using LAS AF software.

Total internal reflection fluorescence (TIRF) microscopic imaging was conducted with a Leica AM TIRF MC total internal reflection fluorescence microscope. A physiological temperature was maintained during the experiments with a temperature control apparatus. Cy3-labeled DNA structures were excited with a 561 nm laser. The fluorescence emission was collected and imaged using a NA = 1.40, 100× oil immersion objective.

Flow cytometric analysis

At least 5000 cells per sample were analyzed in duplicate or triplicate using a FACS Calibur flow cytometer (BD Biosciences, USA). Consistent gating based on cell size and granularity (forward- /side-scattering) was applied to select the fluorescence signals of counted cells.

Dissipative particle dynamics (DPD) simulations

In the simulations, different types of DNA nanostructures that include TDNs with different base pairs (i.e., TDN-13, TDN-20, TDN-32), TDN-20 dimer (i.e., TDN-20d) and six-helix DNA tube with 20 base pairs (i.e., 6-helix) were modeled. Because of the long persistent length (50 nm) of double-stranded DNA, when the length of DNA molecules was short, they were often treated as the rigid rods [5-6]. Besides, some surface beads of the rods carried the charge of -e to ensure that the linear charge density was about 1 e/0.17 nm [6]. When modeling the cell membrane, we firstly used the charge-neutral lipid molecule that consists of a headgroup containing four connected hydrophilic beads and two tails with respective three hydrophobic beads to self-assemble into lipid bilayers, where the first head bead carries a charge of +e, the second head bead carries a charge of -e, and the remaining two beads are uncharged [7]. Besides, experimental results have shown that there are more anionic molecules abundant on the surface of cancer cells as compared to normal cells [8]. To mimic the negative charge property of cancer cells, here for the sake of simplicity, we set some lipid molecules as negatively charged ones in our simulations [9]. And when modeling the negatively charged lipids, non-charged hydrophilic bead was used to replace the first positively charged bead in lipid molecule [9-10]. Moreover, we also used a simplified model to simulate the receptors on the membrane [10-11], where the receptor molecule had the same conformation of

lipid molecule, but its first two head beads were uncharged and can interact with the DNA nanostructures via soft Lennard-Jones (LJ) potentials [12]. Since here we focus on the lipid raft region where the receptors are enriched, the ratio of receptors to lipids in the membrane was set to 0.50 (unless otherwise stated) in order to study the cellular uptake that was not receptor-limited.

The dissipative particle dynamics (DPD) is a coarse-grained simulation technique with hydrodynamic interaction [13]. The dynamics of the elementary units which are so-called DPD beads, is governed by Newton's equation of motion $d\mathbf{v}_i / dt = \mathbf{f}_i / m$. Typically, in the DPD, there are three types of pairwise forces acting on bead i by bead j: the conservative force, dissipative force, and random force. In the present work, the electrostatic force is introduced to take into account the electrostatic interactions between charged beads. The conservative force $\mathbf{F}_{ij}^{C} = a_{ij}(1 - r_{ij} / r_c)\hat{\mathbf{e}}_{ij}$ is used to model the repulsive interaction of beads i and j, where $r_{ij} = |\mathbf{r}_{ij}|$ is the distance between beads i and j, $\hat{\mathbf{e}}_{ij} = \mathbf{r}_{ij} / r_{ij}$ is the unit vector, r_c is the cutoff radius of the force, and a_{ij} represents the maximum repulsion interaction of beads i and j. For any two beads of the same type, we take the repulsive parameter $a_{ii} = 25k_BT / r_C$, and for any two beads of different types, we set the interaction parameter $a_{WH} = a_{WD} = a_{WR} = a_{HD} = a_{HR} = a_{RD} = 25k_BT / r_C$ and $a_{WT} = a_{DT} = a_{HT} = a_{RT} = 100k_BT / r_C$ (W stands for water bead, R stands for receptor head bead, H stands for lipid head bead, T stands for lipid tail bead, D stands for the DNA bead) to denote the hydrophilic/hydrophobic property of the beads[14-15]. The dissipative force $\mathbf{F}_{ij}^{D} = -\gamma(1 - r_{ij} / r_c)(\hat{\mathbf{e}}_{ij} \cdot \mathbf{v}_{ij})\hat{\mathbf{e}}_{ij}$ and random force $\mathbf{F}_{ij}^{R} = \sqrt{2\gamma k_BT}(1 - r_{ij} / r_c)\zeta_{ij}\Delta t^{-1/2}\hat{\mathbf{e}}_{ij}$ are for thermostat, where $\mathbf{v}_{ij} = \mathbf{v}_i - \mathbf{v}_j$ is relative velocity between beads i and j, γ is the strength of friction, ζ_{ij} is a symmetric random variable with zero mean and unit variance, and Δt is the time step of simulation [13].

Electrostatic interactions were incorporated into the DPD simulations by Groot [16]. Since soft potential in the DPD allows for the overlap between DPD beads, when the charged DPD beads are modeled, this can lead to the formation of artificial ion pairs and cause the divergence of the electrostatic potential. To

avoid this problem, Groot chose to spread out the charges using the distribution:[16] $\rho_e(r) = 3/\pi r_e^3(1-r/r_e)$ with $r < r_e$, where r_e is the electrostatic smearing radius, and is typically set as $1.6r_c$ (for details of the method, see Ref. 16 in SI). Moreover, in order to mimic the receptor-ligand interaction, we used a modified LJ potential:[12]

$U_{ij}^{LJ} = 4\epsilon\left[\left(\frac{\sigma}{r_{ij}}\right)^{12} - \left(\frac{\sigma}{r_{ij}}\right)^{6}\right] + 0.22\epsilon$, where $r_{ij} \le r_{cut}$, $\sigma = 0.624r_c$, and ò is used to identify the strength of the TDN-receptor interaction (According to the reported physiological range,[17] we fix it to 5 k_BT unless otherwise stated). The cutoff r_{cut} of the potential is the same as that in the DPD (i.e., r_c). Additionally, to guarantee the proper running of the DPD technology, the repulsive force was set to be $25\,k_BT/r_{cut}$ if it was larger than $25\,k_BT/r_{cut}$, therefore this potential becomes "soft". Further, we used a harmonic bond $U_s = k_s(1-r_{i,i+1}/l_0)^2$ (here we chose $k_s = 64$, $l_0 = 0.5r_c$) between the neighboring beads to ensure the integrality of lipids, and inserted a weaker bond ($k_s = 10$, $l_0 = 0.5r_c$) between the first hydrophobic beads on two tails of the lipid to keep the tails oriented in the same direction.[15] We also used a three-body bond angle potential $U_a = k_a(1-cos(\phi-\phi_0))$ to depict the rigidity of lipid tails ($k_a = 10$, $\phi_0 = 180^\circ$).

Our simulations applied the velocity-Verlet integration algorithm and the integration time step $\Delta t = 0.015\tau$. In addition, we chose the cutoff radius r_c, bead mass m, energy k_BT as the simulation units. All simulations were performed in the NVT ensembles. The size of the simulation box was $75r_c \times 75r_c \times 40r_c$ with the number density of $\rho = 3/r_c^3$. The area (A_0) per lipid when the membrane is under zero tension at the beginning of the simulations is about $1.28\,nm^2$. During the simulations, to keep the membrane surface under zero tension, the box shape changed with the area (A_b) per lipid on the boundary, i.e., if $A_b > A_0$, the box would be compressed in X-Y plane until $A_b = A_0$; while if $A_b < A_0$, the box would be stretched in X-Y plane until $A_b = A_0$. At the same time, the box length in

membrane-normal direction would change correspondingly to keep the box volume fixed [14]. And we performed the above operation every 1000 time steps. The periodic boundary conditions were adopted in three directions. We can convert the DPD units into SI units via examining the membrane thickness and the lipid diffusion coefficient.[12] Usually, the thickness of DPPC bilayer is about 4nm and the in-plane diffusion constant of lipids is about $5.0\,\mu m^2/s$ in experiment. Comparing that the thickness is about $4.0\,r_c$ and diffusion constant is about $0.012\,r_c^2/\tau$, we can yield $r_c = 1.0nm$ and $\tau = 2.4ns$. All simulations in this work were carried out by using the modified soft package Lammps (1 Feb 2014).[18]

To calculate the free energy for the interaction of TDN-20 with negatively charged membrane, biased simulations were done by using a harmonic potential with a force constant of 1000 k_BT/r_c^2 applied between them. The separation distance along the Z axis between the mass center of TDN-20 and the central plane of the membrane was from 14.0 nm to 3.0 nm and was divided into 40 windows. The weighted histogram analysis method (WHAM)[19] was then applied to calculate the potential of mean force (PMF) after 3.6 μs of simulation for each window.

References

(1) Goodman, R. P.; Schaap, I. A.; Tardin, C. F.; Erben, C. M.; Berry, R. M.; Schmidt, C. F.; Turberfield, A. J. Rapid chiral assembly of rigid DNA building blocks for molecular nanofabrication. *Science* **2005,** *310,* 1661-1665.

(2) Wang, T.; Schiffels, D.; Cuesta, S. M.; Fygenson, D. K.; Seeman, N. C. Design and characterization of 1D nanotubes and 2D periodic arrays self-assembled from DNA multi-helix bundles. *J. Am. Chem. Soc.* **2012,** *134,* 1606-1616.

(3) Kim, J. A.; Aberg, C.; Salvati, A.; Dawson, K. A. Role of cell cycle on the cellular uptake and dilution of nanoparticles in a cell population. *Nat. Nanotechnol.* **2012,** *7,* 62-68.

(4) Gutierrez, M. G.; Master, S. S.; Singh, S. B.; Taylor, G. A.; Colombo, M. I.; Deretic, V. Autophagy is a defense mechanism inhibiting BCG and Mycobacterium tuberculosis survival in infected macrophages. *Cell* **2004,** *119,* 753-766.

(5) Brinkers, S.; Dietrich, H. R. C.; Groote, F. H. d.; Young, I. T.; Rieger, B. The persistence length of

double stranded DNA determined using dark field tethered particle motion. *J. Chem. Phys.* **2009,** *130,* 215105.

(6) Farago, O.; Grønbech-Jensen, N. Simulation of self-assembly of cationic lipids and DNA into structured complexes. *J. Am. Chem. Soc.* **2009,** *131,* 2875-2881.

(7) Izvekov, S.; Voth, G. A. A multiscale coarse-graining method for biomolecular systems. *J. Phys. Chem. B* **2005,** *109,* 2469-2473.

(8) Jobin, M. L.; Alves, I. D. On the importance of electrostatic interactions between cell penetrating peptides and membranes: A pathway toward tumor cell selectivity? *Biochimie* **2014,** *107,* 154-159.

(9) Ding, H. M.; Ma, Y. Q. Design maps for cellular uptake of gene nanovectors by computer simulation. *Biomaterials* **2013,** *34,* 8401-8407.

(10) Ding, H. M.; Ma, Y. Q. Computer simulation of the role of protein corona in cellular delivery of nanoparticles. *Biomaterials* **2014,** *35,* 8703-8710.

(11) Shi, X.; von dem Bussche, A.; Hurt, R. H.; Kane, A. B.; Gao, H. Cell entry of one-dimensional nanomaterials occurs by tip recognition and rotation. *Nat. Nanotechnol.* **2011,** *6,* 714-719.

(12) Yang, K.; Ma, Y. Q. Computer simulation of the translocation of nanoparticles with different shapes across a lipid bilayer. *Nat. Nanotechnol.* **2010,** *5,* 579-583.

(13) Groot, R. D.; Warren, P. B. Dissipative particle dynamics: Bridging the gap between atomistic and mesoscopic simulation. *J. Chem. Phys.* **1997,** *107,* 4423-4435.

(14) Smith, K. A.; Jasnow, D.; Balazs, A. C. Designing synthetic vesicles that engulf nanoscopic particles. *J. Chem. Phys.* **2007,** *127,* 084703.

(15) Ding, H. M.; Tian, W. D.; Ma, Y. Q. Designing nanoparticle translocation through membranes by computer simulations. *ACS Nano* **2012,** *6,* 1230-1238.

(16) Groot, R. D. Electrostatic interactions in dissipative particle dynamics-simulation of polyelectrolytes and anionic surfactants. *J. Chem. Phys.* **2003,** *118,* 11265-11277.

(17) Pierre, B. Ligand-receptor interactions. *Rep. Prog. Phys.* **1999,** *62,* 921.

(18) Plimpton, S. Fast parallel algorithms for short-range molecular dynamics. *J. Comput. Phys.* **1995,** *117,* 1-19.

(19) Roux, B. The calculation of the potential of mean force using computer simulations. *Comput. Phys. Commun.* **1995,** *91,* 275-282.

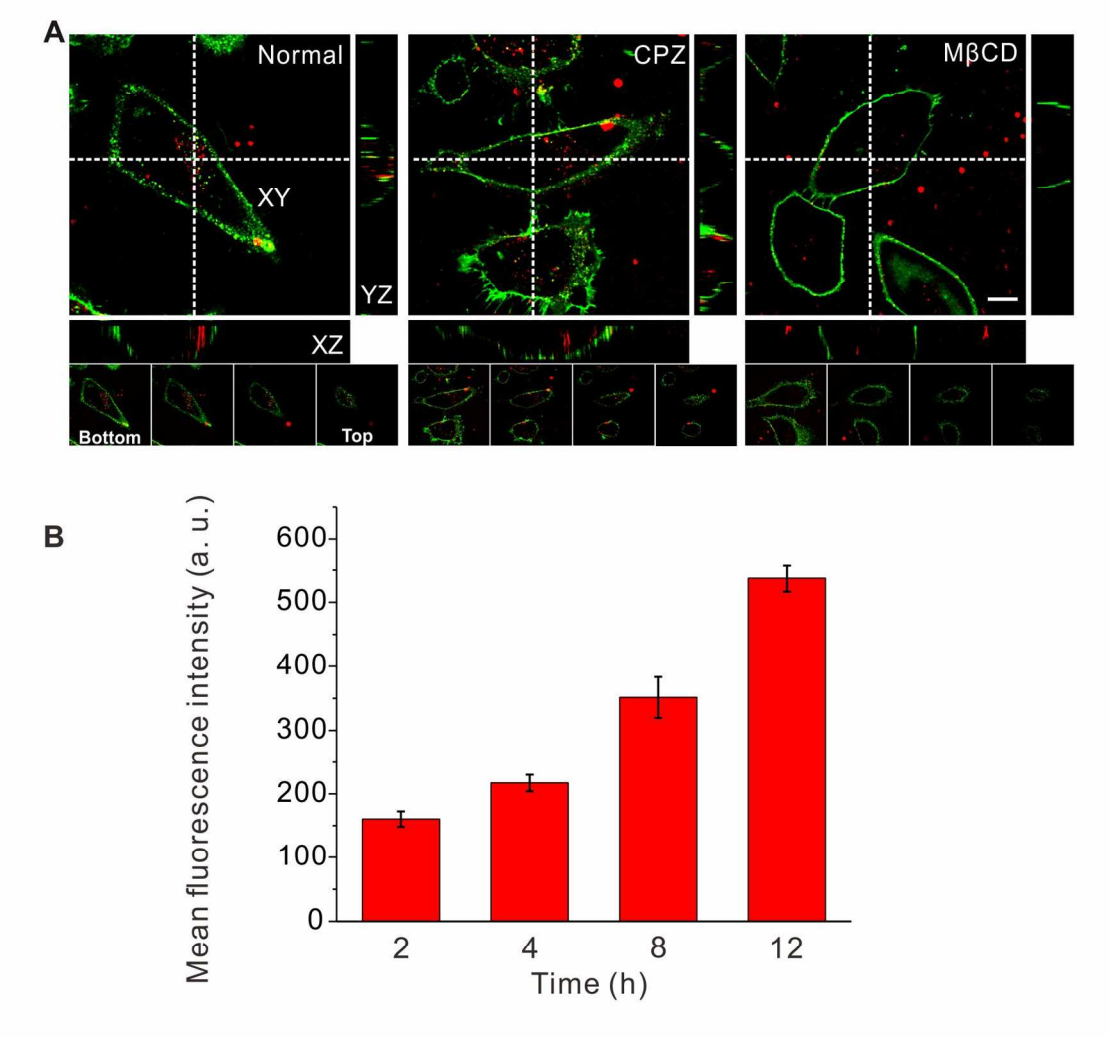

Figure S1. TDN-20 internalized by living cells. (A) 3D confocal images colocalizing TDN-20 (red) and cell membrane (green) under 37˚C without inhibitor (Normal), or with CPZ, or MβCD. (B) Flow cytometric results showing fluorescence of TDN-20 in cells upon time. The fluorescence intensity was subtracted with which from cells without TDN-20 treatment.

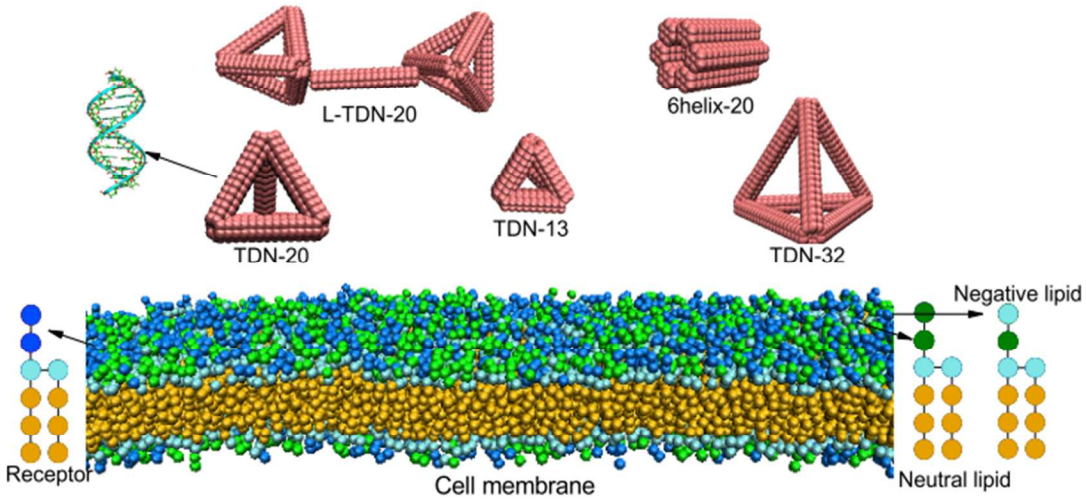

Figure S2. Schematic illustration of the model system in the simulations. The green bead represents charged head in lipid molecule (the first green bead containing +*e* and the second one containing -*e*), while lime bead stands for lipid hydrophilic bead (without charge), and the orange bead represents lipid tail. The pink bead represents the DNA nanostructures (TDN-13, TDN-20, TDN-32, TDN-20d, 6-helix). Water and ion beads are not shown for clarity.

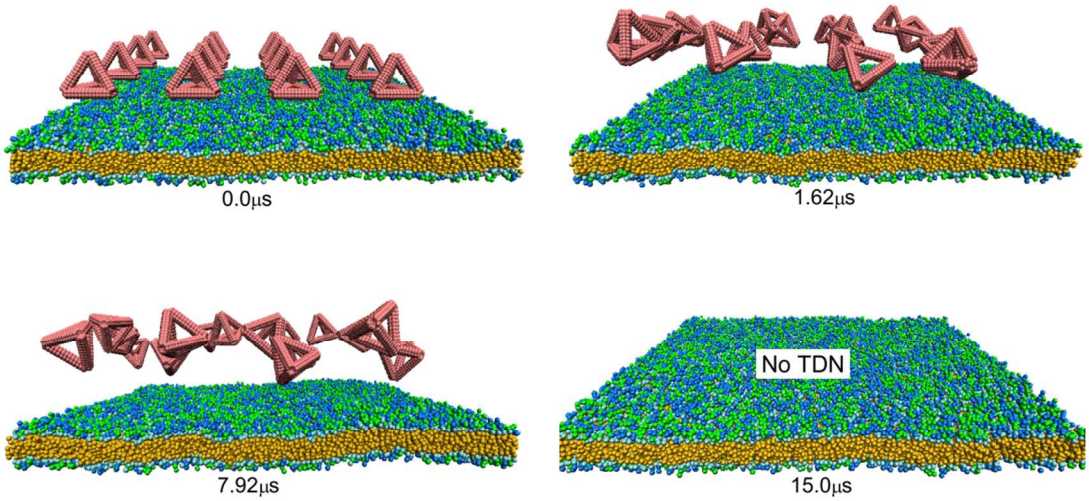

Figure S3. Simulated interactions between TDN-20 and the membrane without attraction from lipid raft proteins.

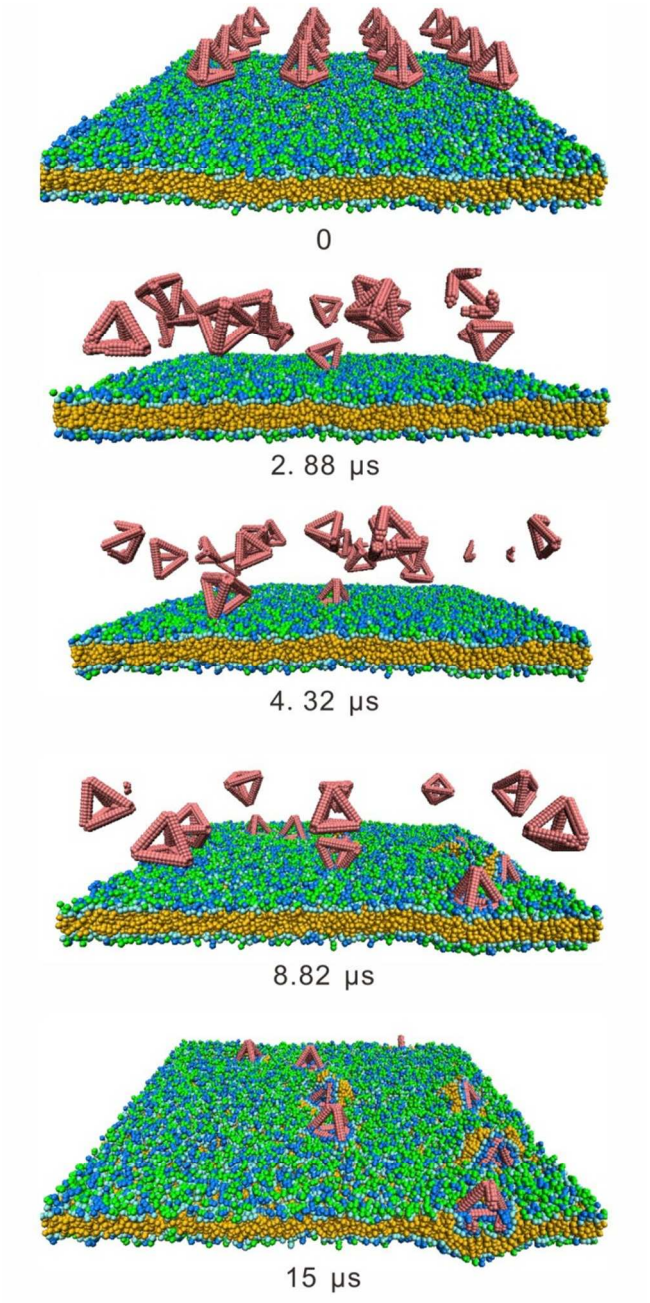

Figure S4. Simulated interactions between TDN-20 and the membrane with attraction from lipid raft proteins.

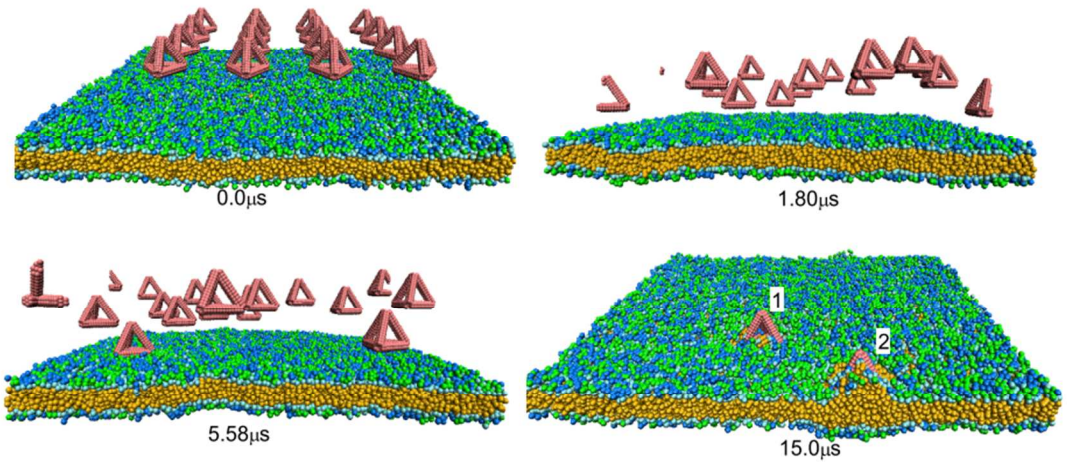

Figure S5. Simulated interactions between rotation-constrained TDN-20 and the cell membrane.

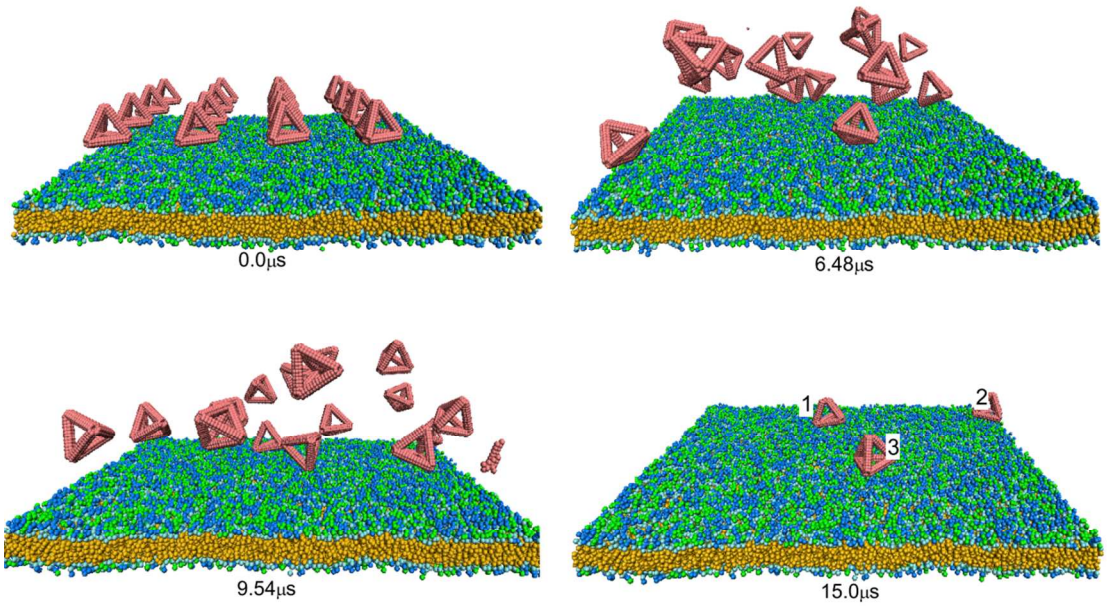

Figure S6. Simulated interactions between TDN-20 structures and frozen membrane.

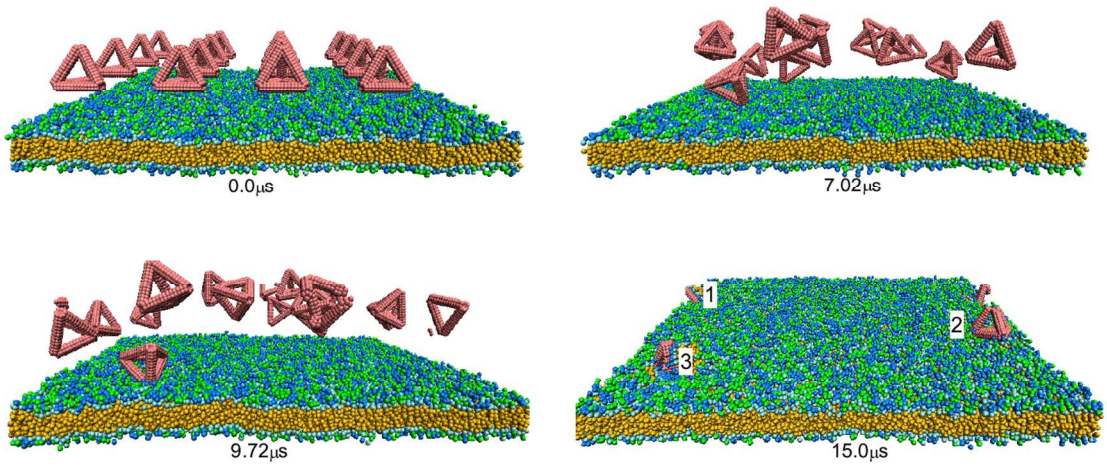

Figure S7. Time evolution of simulated interaction between TDN-20 structures and more negatively charged cell membrane. Average surface charge density, -0.08 e/nm^2. Only 3 of the 16 TDN-20 structures touched the cell membrane within 15 μs.

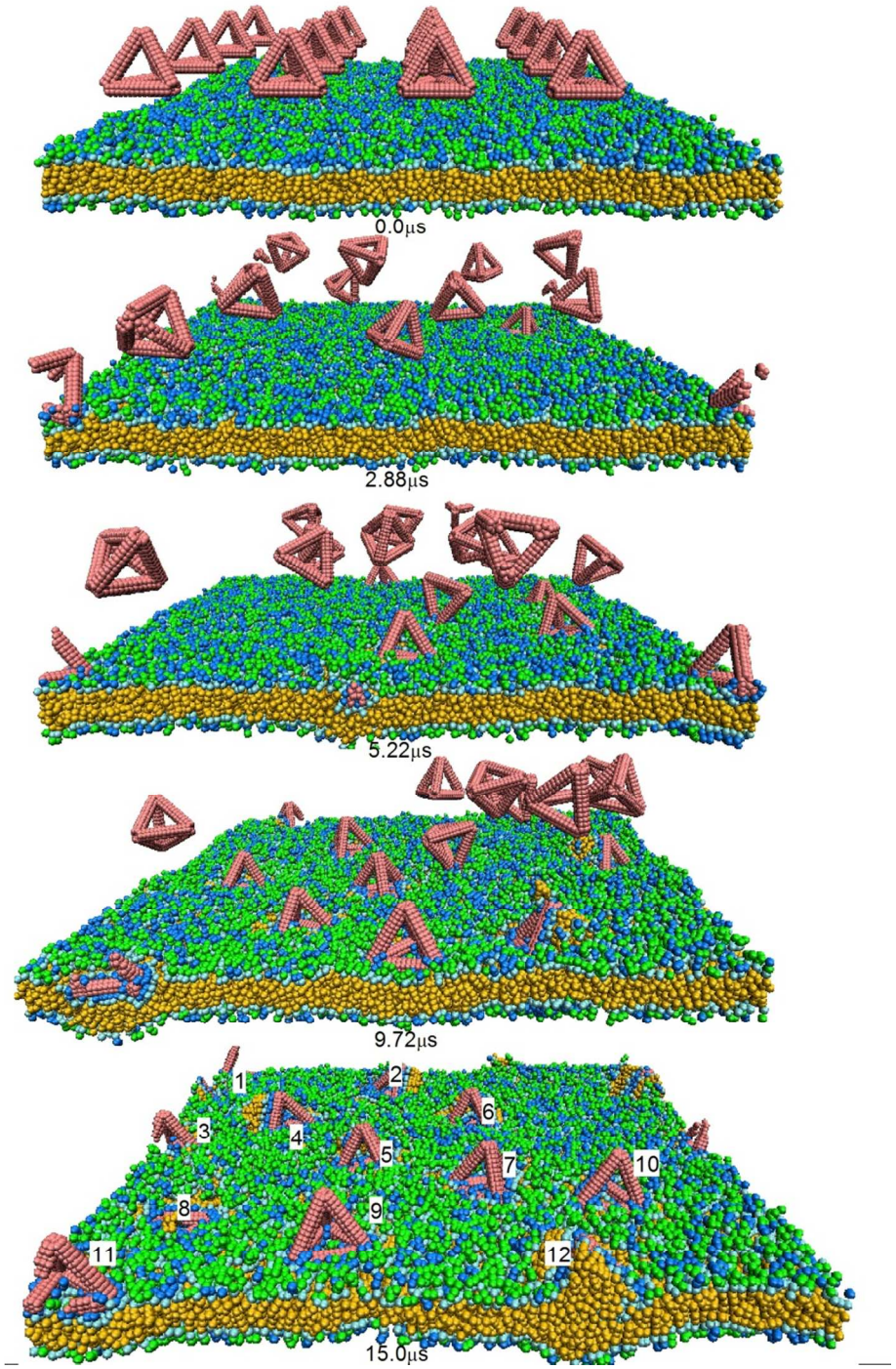

Figure S8. Time evolution of simulated interaction between TDN-20 structures and neutrally charged cell membrane. Average surface charge density, 0 e/nm^2. 12 of the 16 TDN-20 structures touched the cell membrane within 15 μs.

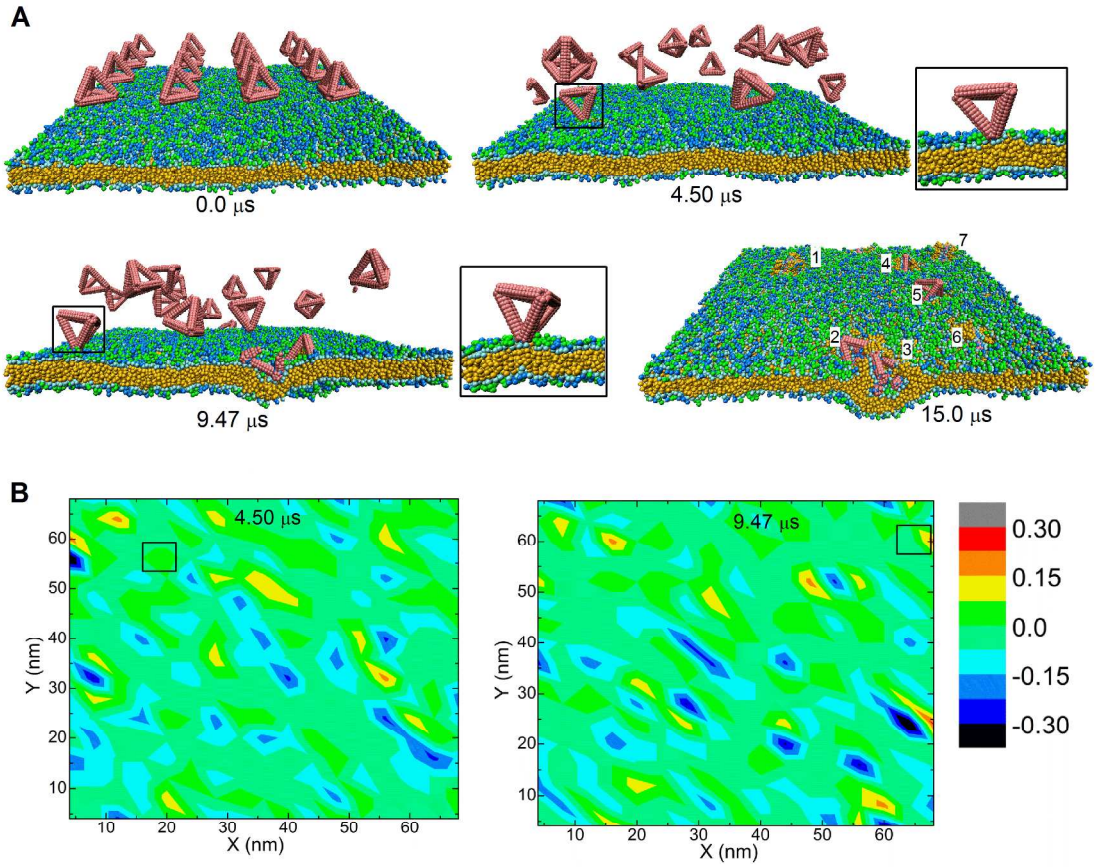

Figure S9. (A) Time evolution of simulated interaction between TDN-20 structures and negatively charged cell membrane, where the strength of short-range attraction is 10.0 k_BT. Most of the adsorbed TDN-20 structures could be engulfed by the membrane within 15 μs due to the strong attractive interaction. (B) Representative landing spots of the structures on the cell membrane in typical simulations.

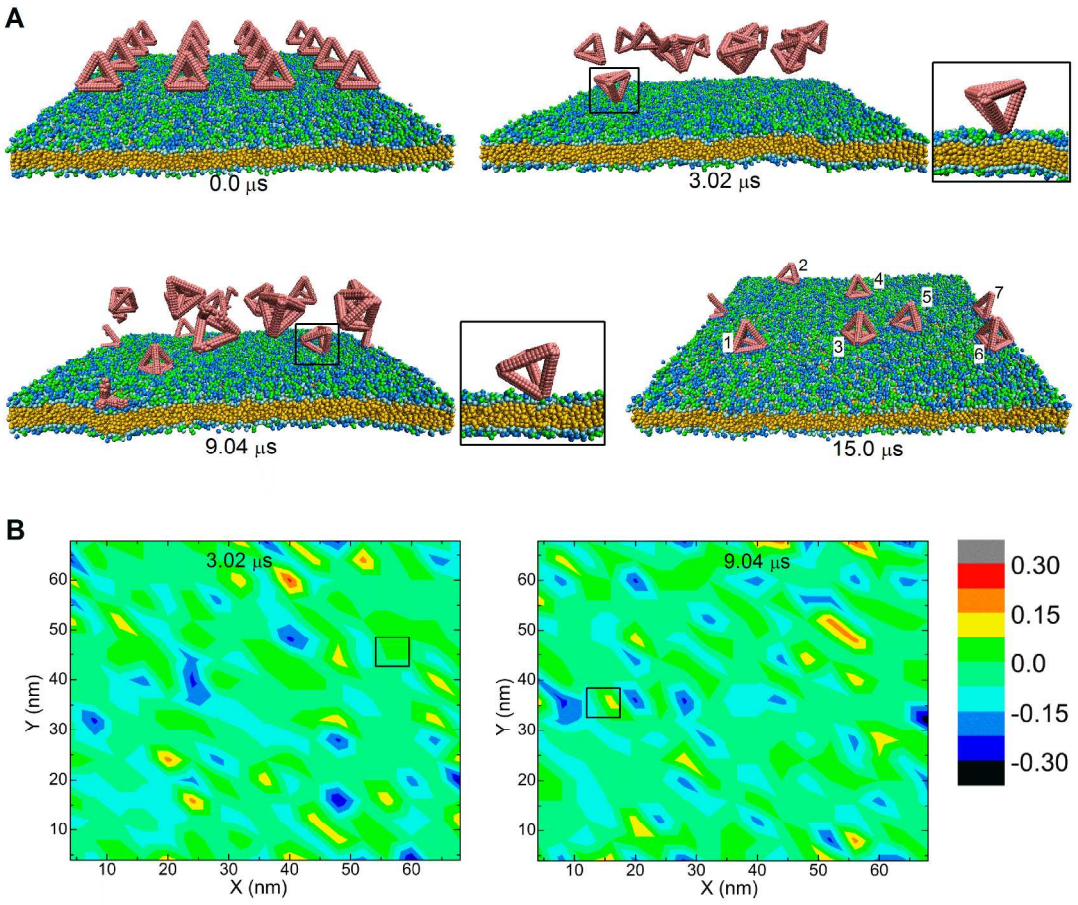

Figure S10. (A) Time evolution of simulated interaction between TDN-20 structures and negatively charged cell membrane, where the strength of short-range attraction is 2.5 k_BT. Since the weak attraction here cannot balance out the bending energy of membrane deformation, all of the adsorbed TDN-20 structures were still attached on the cell membrane within 15 μs. (B) Representative landing spots of the structures on the cell membrane in typical simulations.

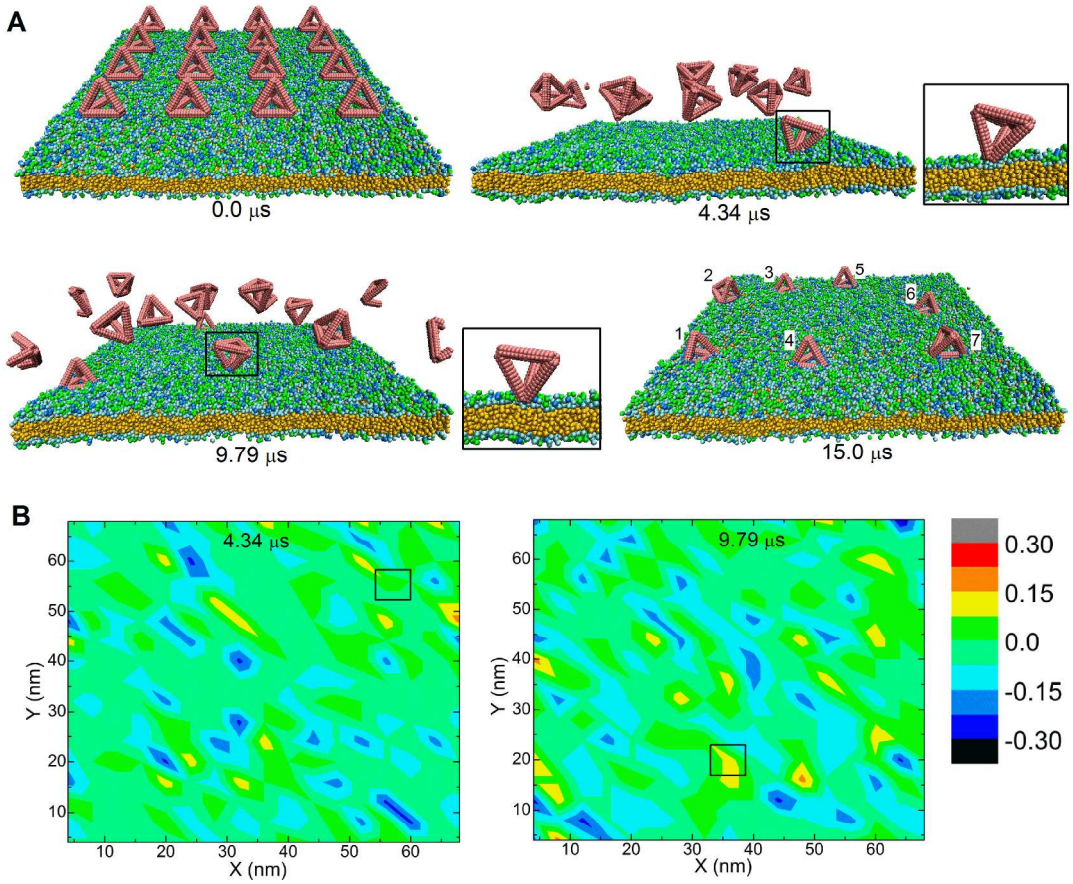

Figure S11. (A) Time evolution of simulated interaction between TDN-20 structures and negatively charged cell membrane. The ratio of receptors in the membrane is 0.25. Due to the lack of receptors, the adsorbed TDN-20 structures cannot be effectively engulfed by the membrane within 15 μs. (B) Representative landing spots of the structures on the cell membrane in typical simulations.

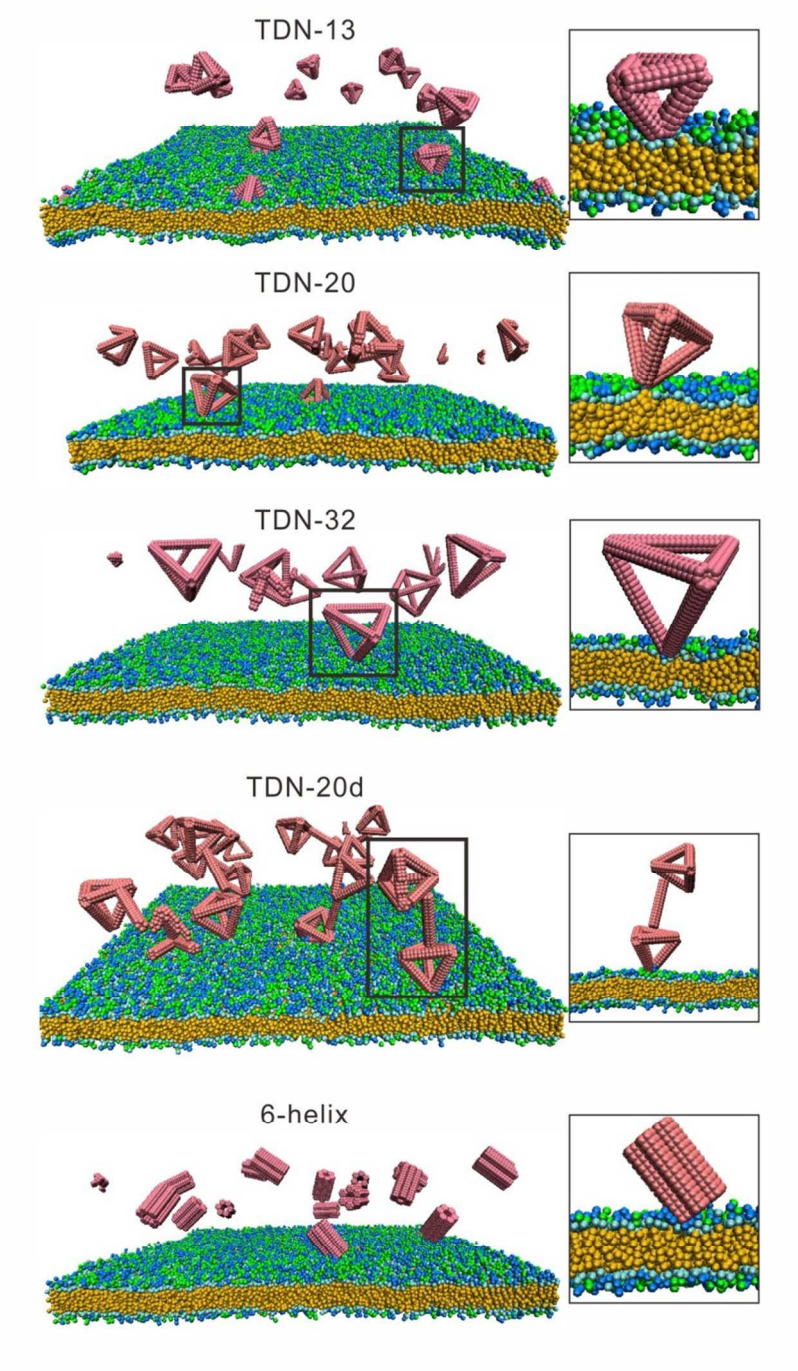

Figure S12. Different DNA nanostructures touching the cell membrane in the corner attack approach.

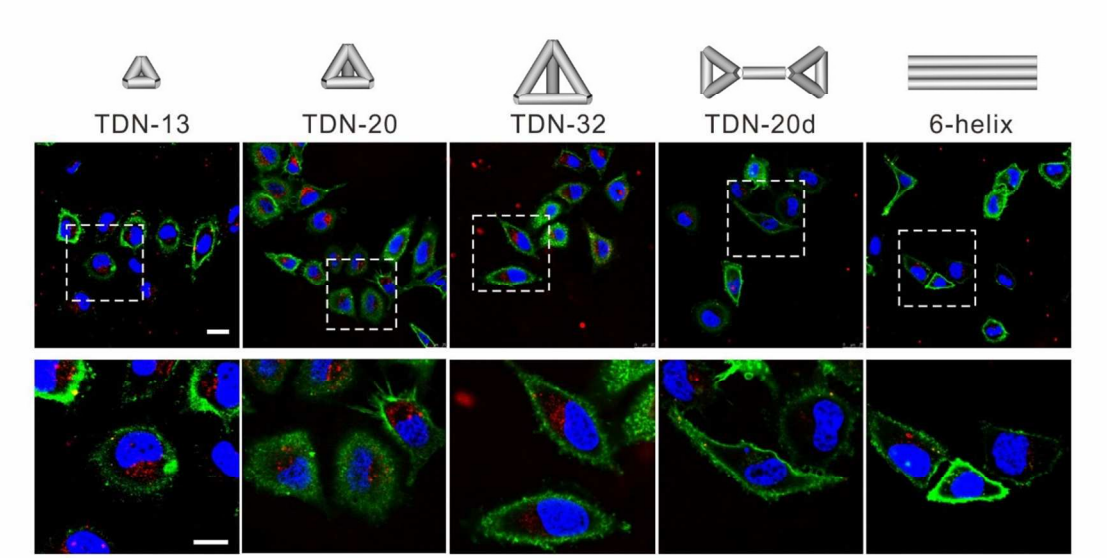

Figure S13. Confocal fluorescence microscopic images showing DNA nanostructures internalized by the HeLa cells. Red, DNA nanostructures; green, cell membrane; blue, cell nuclei. The lower images are zoom in from the selected regions of the upper ones. Scale bar: 10 μm.

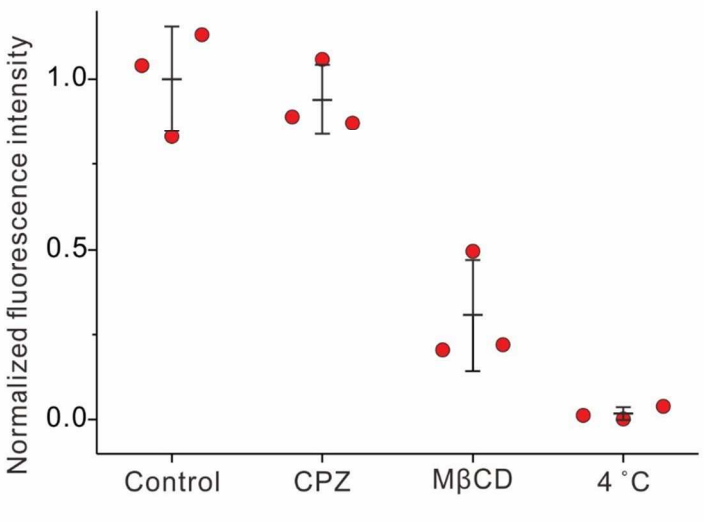

Figure S14. Flow cytometric fluorescence analysis of HeLa cells fed with TDN-20d under different inhibitor treatments.

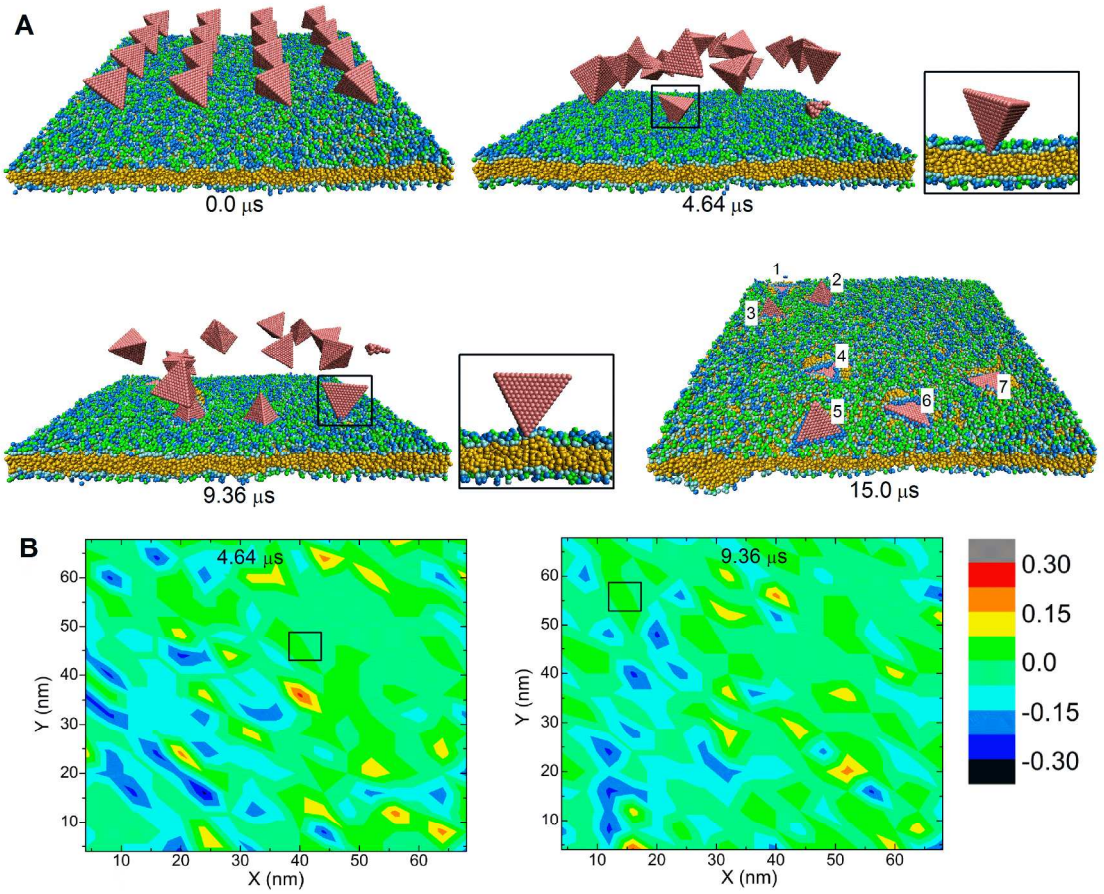

Figure S15. (A) Time evolution of simulated interaction between anionic triangular pyramid nanoparticles and negatively charged cell membrane. (B) Representative landing spots of the nanoparticles on the cell membrane in typical simulations.

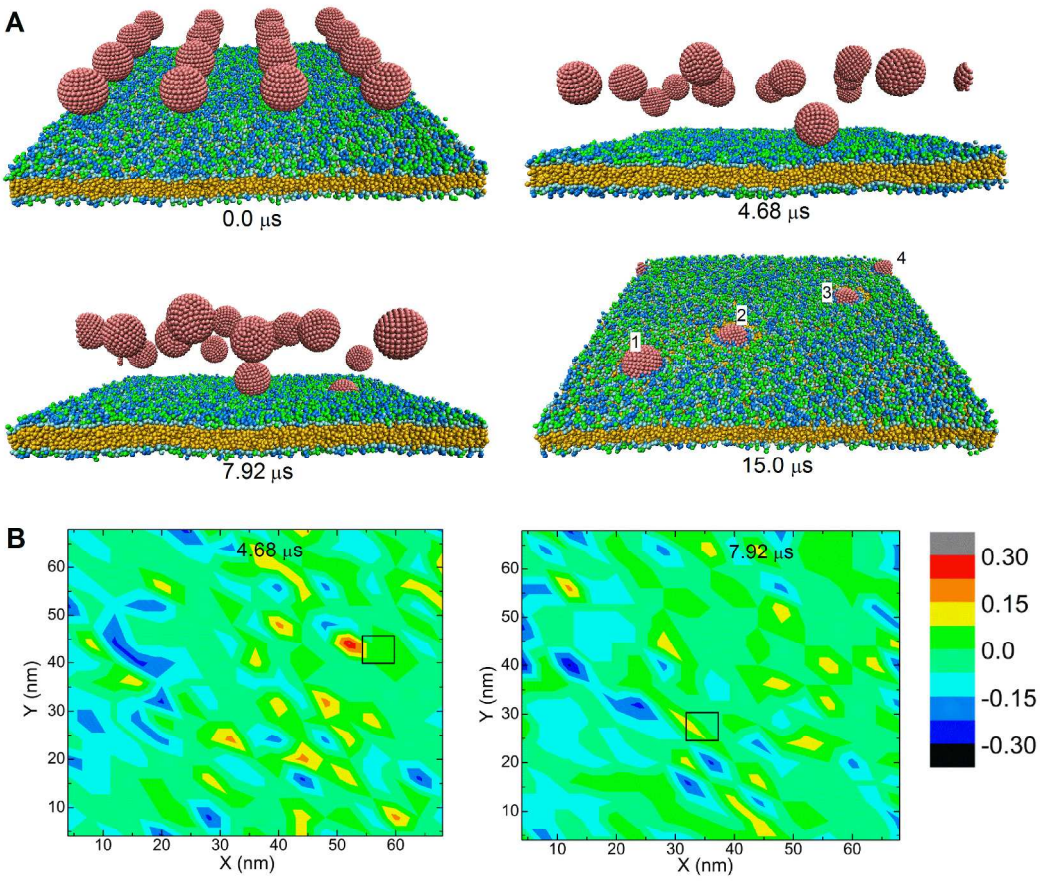

Figure S16. (A) Time evolution of simulated interaction between anionic sphere nanoparticles and negatively charged cell membrane. (B) Representative landing spots of the nanoparticles on the cell membrane in typical simulations.

Table S1. Sequences of oligonucleotides.

Sequence ID	Sequence (5'-3')
TDN-13-S1	ACACTACGTCAGAACAGCTTGCATCACTGGTCACCAGAGTA-Cy3
TDN-13-S2	ACGAGCGAGTTGATGTGATGCAAGCTGAATGCGAGGGTCCT-Cy3
TDN-13-S3	TCAACTCGCTCGTAACTACACTGTGCAATACTCTGGTGACC-Cy3
TDN-13-S4	TCTGACGTAGTGTATGCACAGTGTAGTAAGGACCCTCGCAT-Cy3
TDN-20-S1	CAGTTGAGACGAACATTCCTAAGTCTGAAATTTATCACCCGCCA TAGTAGACGTATCACCAGG-Cy3
TDN-20-S2	CTTGCTACACGATTCAGACTTAGGAATGTTCGACATGCGAGGGT CCAATACCGACGATTACAG-Cy3
TDN-20-S3	GGTGATAAAACGTGTAGCAAGCTGTAATCGACGGGAAGAGCAT GCCCATCCACTACTATGGCG-Cy3
TDN-20-S4	CCTCGCATGACTCAACTGCCTGGTGATACGAGGATGGGCATGCT CTTCCCGACGGTATTGGAC-Cy3
TDN-32-S1	CCCGATAGTTGATCACACGCCACCCCTTTCCATTGCATGCGCGCT GGTGAAACGACTGCCGGCCCATCTCATACTGGAGGCGATTACCT GGGCCTGGGC-Cy3
TDN-32-S2	TGCGCTCCGGTAATAGACACCAGCGCGCATGCAATGGAAAGGG GTGGCGATCCGACGGACCTCGCATTCTTCGCACCCTCGAAGCCC TGGGGCGGTACT-Cy3
TDN-32-S3	TGCGAGGTCCGTCGGAaGTGATCAACTATCGGGGCCCAGGCCCA GGTAAAAAGAACAGTGTTcTGGGGAACACAGCCTGACTATCGAG GGTGCGAAGAA-Cy3
TDN-32-S4	CCAGAACACTGTTCTTACGCCTCCAGTATGAGATGGGCCGGCAG TCGTTACTATTACCGGAGCGCAAGTACCGCCCCAGGGCAAGTCA GGCTGTGTTCC-Cy3

6-helix-S1	CAGTTGACTGCTAGTACCTGAGCACTGAATGCGATGTAGAAGTA GCTCTGCTCCATC
6-helix-S2	CGACTTGATGGAGCAGACCTATCGTCAC
6-helix-S3	AGGCAGATACGAAGAGCGAGGCTATGTCGTAGATAGTTCTCGC ACGACGCTAGACAC
6-helix-S4	GCAGTCAACTG
6-helix-S5	CGGTACGTGACGATAGGACACATCAGATGTCTTAGGAGAGGTC ACAGTAACCTTCGACAATCT
6-helix-S6	AGATTGTCGAACGTATCTGCCT
6-helix-S7	GATGCGTGAACTATGACATCTGATGTGTGCTACTTGTCACCA
6-helix-S8	TCGAGTACGCTCTTGGTTACTGTGACCTGTGCTCACGAGGAC
6-helix-S9	GCATTCACTCCTAACTACGAC-Cy3
6-helix-S10	TCTAGCGTGTCTAGCGT-Cy3
6-helix-S11	TGTCCGTGCAACCGATCAATCC
6-helix-S12	GCCTAGCGATCCAATGGAACGACCGTATTGCTGAGGTGAGTGTA TGTATCACTTGCACGGACA
6-helix-S13	CTGTACCGTTG
6-helix-S14	GGATTGATCGGATGCCAGACGCATCGGATTCGATGAGCCTACTC GACCAACTCAACG
6-helix-S15	GGCAATGTCCACCATTGGATCG
6-helix-S16	CAACGGTACAGTGGTGACTCCAACCTTGTAACGTCCTCGATAAC GCTGGACATTGCC
6-helix-S17	CGTGCGACTGGCATGTGATACATACACTGGTTGGACTACATC
6-helix-S18	ATAGCCTGGCTCATGCAATACGGTCGTTGCGTTATGGTACTA
6-helix-S19	GTTACAACACCTCACGAATCC-Cy3
6-helix-S20	GCACCACGTTGAGTTGG-Cy3

To make different DNA nanostructures equivalent in fluorescence intensity, each structure had four component oligonucleotides labeled with Cy3 at the 3’ ends.